

## **Radiocarbon and $^{230}\text{Th}$ data reveal rapid redistribution and temporal changes in sediment focussing at a North Atlantic drift**

Gesine Mollenhauer<sup>a,b,\*</sup>, Jerry F. McManus<sup>c,d</sup>, Thomas Wagner<sup>e</sup>, I. Nick McCave<sup>f</sup>, Timothy I. Eglinton<sup>c</sup>

<sup>a</sup> Alfred-Wegener-Institute for Polar and Marine Research, Am Handelshafen 12, 27570 Bremerhaven, Germany (Gesine.Mollenhauer@awi.de)

<sup>b</sup> Department of Geosciences, University of Bremen, Klagenfurter Str., 28359 Bremen, Germany

<sup>c</sup> Woods Hole Oceanographic Institution, Woods Hole, MA 02543, USA (teglinton@whoi.edu)

<sup>d</sup> now at: Lamont-Doherty Earth Observatory, Palisades, NY 10964-8000, USA (jmcmanus@ldeo.columbia.edu)

<sup>e</sup> School of Civil Engineering and Geosciences, Newcastle University, Newcastle upon Tyne, NE1 7RU, UK (thomas.wagner@ncl.ac.uk)

<sup>f</sup> Department of Earth Sciences, University of Cambridge, Cambridge, CB2 3EQ, U.K (mccave@esc.cam.ac.uk)

\* corresponding author; Telephone: +49-421-218 65070, Fax: +49-421-218 8942

1 **Abstract**

2 In locations of rapid sediment accumulation receiving substantial amounts of laterally  
3 transported material the timescales of transport and accurate quantification of the  
4 transported material are at the focus of intense research. Here we present radiocarbon  
5 data obtained on co-occurring planktic foraminifera, marine haptophyte biomarkers  
6 (alkenones) and total organic carbon (TOC) coupled with excess Thorium-230 ( $^{230}\text{Th}_{\text{xs}}$ )  
7 measurements on four sediment cores retrieved in 1649-2879 m water depth from two  
8 such high accumulation drift deposits in the Northeast Atlantic, Björn and Gardar Drifts.  
9 While  $^{230}\text{Th}_{\text{xs}}$  inventories imply strong sediment focussing, no age offsets are observed  
10 between planktic foraminifera and alkenones, suggesting that redistribution of  
11 sediments is rapid and occurs soon after formation of marine organic matter, or that  
12 transported material contains negligible amounts of alkenones. An isotopic mass  
13 balance calculation based on radiocarbon concentrations of co-occurring sediment  
14 components leads us to estimate that transported sediment components contain up to  
15 12% of fossil organic matter that is free of or very poor in alkenones, but nevertheless  
16 appears to consist of a mixture of fresh and eroded fossil material. Considering all  
17 available constraints to characterize transported material, our results show that  
18 although focussing factors calculated from bulk sediment  $^{230}\text{Th}_{\text{xs}}$  inventories may allow  
19 useful approximations of bulk redeposition, they do not provide a unique estimate of the  
20 amount of each laterally transported sediment component. Furthermore, our findings  
21 provide evidence that the occurrence of lateral sediment redistribution alone does not  
22 always hinder the use of multiple proxies but that individual sediment fractions are  
23 affected to variable extents by sediment focussing.

24

25 **Keywords:** compound-specific radiocarbon dating, alkenones,  $^{230}\text{Th}_{\text{xs}}$ . focussing factors,  
26 drift sediments

27

## 28 **1) Introduction**

29 Marine sediments accumulating at high rates represent a valuable archive of  
30 information on the variability of environmental conditions in the past. High temporal  
31 resolution records of climate variability are of particular importance in context of  
32 growing awareness of Earth's potential for abrupt and dramatic climate change. The  
33 search for high resolution sediments has driven paleoclimate research to focus on the  
34 flanks of the ocean basins, where enhanced biological productivity and delivery of  
35 terrigenous materials lead to high rates of sediment accumulation, and on drifts where  
36 deposition of hemipelagic sediments is focussed by bottom currents and topography  
37 (Flood and Hollister, 1974; McCave and Tucholke, 1986). At these drift sites, fine-  
38 grained material, possibly from distal locations, serves as a diluent that expands the  
39 depth-time axis facilitating high temporal resolution paleoclimate reconstruction.  
40 However, this high resolution may come at the price of a more complicated  
41 sedimentological history that needs to be unraveled to appraise the full potential of  
42 these unique sediments (McCave, 2002).

43 In recent years, a growing number of paleoenvironmental reconstructions have  
44 documented the widespread occurrence of sediment redistribution processes in  
45 different sedimentological settings (e.g., Kienast et al., 2007; Marcantonio et al., 2001;  
46 Turnewitsch et al., 2008). Evidence for lateral transport comes from a range of different  
47 approaches, including sediment trap studies (Thomsen et al., 1998), constant-flux  
48 proxies such as Helium-3 ( $^3\text{He}$ ) and excess Thorium-230 ( $^{230}\text{Th}_{\text{xs}}$ ) (Marcantonio et al.,

49 2001), and radiocarbon dating of co-occurring coarse and fine-grained sedimentary  
50 constituents (Ohkouchi et al., 2002).

51 Lateral displacement of sediment by currents generally involves sorting of particles  
52 according to their hydrodynamic behaviour. As a consequence, selective lateral  
53 transport can therefore lead to de-coupling of paleoenvironmental records deduced  
54 from different particle types and size classes, notably those using relatively coarse-  
55 grained foraminiferal shells and organic matter (e.g., molecular proxies.  $\delta^{15}\text{N}$ ) residing  
56 predominantly in the fine fraction. If transport occurs over long distances, the associated  
57 proxy records might not be representative of local environmental conditions (McCave,  
58 2002).

59 Compound-specific radiocarbon dating has revealed that, in some locations affected  
60 by lateral transport, fine-grained organic matter may be substantially pre-aged by the  
61 time of deposition (Mollenhauer et al., 2003; Mollenhauer et al., 2005; Ohkouchi et al.,  
62 2002). The resulting age offsets between fine-grained material containing a substantial  
63 amount of transported particles and coarse-grained, predominantly locally formed  
64 sediment constituents are particularly pronounced at Bermuda Rise, a North Atlantic  
65 sediment drift site (Ohkouchi et al., 2002). As a consequence, great concern was raised  
66 regarding the reliability of palaeoenvironmental reconstructions at drift sites using  
67 biomarkers or other proxies associated with the sediment fine fraction (McCave, 2002).  
68 However, in other locations known to be affected by lateral sediment redistribution,  
69 age-offsets between fine-grained and coarse-grained sediment particles are negligible  
70 (Kusch et al., 2010; Mollenhauer et al., 2006).

71 The timescales of sediment redistribution and the effects on palaeoenvironmental  
72 information appear to be different and strongly dependent on the local sedimentological  
73 regime. The composition of sediments in the source region, the local topography

74 (Turnewitsch et al., 2008), and. to a more limited extent restricted mostly to continental  
75 margins, the depth at which transport occurs (surface vs. deep ocean currents), among  
76 other factors, are potentially controlling parameters. In order to develop a predictive  
77 capability of whether a proxy record obtained at a high-accumulation rate site is likely  
78 biased by transported and pre-aged material, it is essential to understand these  
79 controlling parameters.

80 Here we present a new data set from a Northeast Atlantic sediment drift, including  
81 excess  $^{230}\text{Th}$  data and radiocarbon ages of co-occurring planktic foraminifera, total  
82 organic matter (TOC) and marine phytoplankton-derived alkenones. Our results show  
83 that differences in sediment focussing result in variable age offsets between  
84 foraminifera and total organic carbon, implying the addition of pre-aged transported  
85 organic matter. However, unlike at Bermuda Rise, age offsets between marine  
86 phytoplankton-derived biomarkers and planktic foraminifera are small or negligible.  
87 Furthermore, the age offset between total organic matter and planktic foraminifera is  
88 variable and increases considerably during the last glacial, implying changes in  
89 composition of laterally advected sediments and in its source area.

90

## 91 **2) Study area and sediment cores**

92 Our study area is located in the Iceland Basin in the Northeast Atlantic Ocean.  
93 Within this basin, Iceland-Scotland Overflow water flowing from NE to SW as a Deep  
94 Western Boundary Current, results in the formation of large-scale sediment drifts. Björn  
95 Drift and Gardar Drift form on the southeastern flank of the Reykjanes Ridge and in the  
96 central Iceland Basin, respectively. These sediments consist of material remobilized  
97 from the SE Iceland slope (Bianchi and McCave, 2000). Sedimentation rates vary  
98 strongly depending on the local current regime and reach values as high as  $120 \text{ cm ka}^{-1}$ .

99 We used sediment samples from ODP Site 984A and 984C drilled during Leg 162  
100 on Björn Drift in about 1650 m water depth (Jansen et al., 1996). Additional sediments  
101 from three box cores (NEAP5B, 11B and 18B; 38cm, 39cm, and 37cm length,  
102 respectively) recovered during RRS Charles Darwin cruise 88 (McCave, 1994) were  
103 investigated (Table 1; Figure 1). The locations were chosen on and off the axis of  
104 accumulation of the drifts as manifested by the thickness of Holocene sediments at the  
105 respective sites (Bianchi and McCave, 2000).

106

### 107 **3) Methods**

#### 108 *Radiocarbon analyses*

109 Radiocarbon dating was performed at the National Ocean Sciences Accelerator  
110 Mass Spectrometry (NOSAMS) facility at the Woods Hole Oceanographic Institution,  
111 USA. Accelerator mass spectrometer (AMS) radiocarbon ages were determined on TOC  
112 and planktic foraminifera for each core-top and core-bottom box core sample.  
113 Radiocarbon ages of TOC and planktic foraminifera were also obtained for six depth  
114 intervals of ODP core 984A (Table 2). Additional TOC and foraminifera radiocarbon  
115 analyses were performed on ODP 984C. These analyses were done using standard  
116 procedures for TOC and foraminifera (McNichol et al., 1994). Briefly, subsamples of  
117 homogenized bulk sediments containing approximately 1 mg of organic carbon were  
118 hydrolyzed with 10% hydrochloric acid and combusted in evacuated, pre-combusted  
119 quartz tubes with copper oxide and silver. Resulting carbon dioxide (CO<sub>2</sub>) was purified  
120 and graphitized over an iron catalyst; graphite targets were then pressed for AMS  
121 analysis. Aliquots of CO<sub>2</sub> gas were used for stable carbon isotopic determination using a  
122 VG Prism mass spectrometer. Planktic foraminifera were picked from the >150 µm  
123 fraction of wet-sieved subsamples of solvent-extracted sediment residues. For each  
124 sample, the most abundant shallow-dwelling species was chosen (*G. bulloides* in

125 Holocene sediments, *N. pachyderma* in glacial section; Table 2). Foraminifera samples  
126 were hydrolyzed in phosphoric acid, and resulting CO<sub>2</sub> gas was treated as described  
127 above.

128 Abundance permitting, molecular-level radiocarbon dates were obtained on  
129 alkenones as a compound class (C<sub>37</sub>, C<sub>38</sub>, and C<sub>39</sub> alkenones). Samples containing  
130 sufficient alkenones for radiocarbon analyses included those from the Holocene section  
131 of ODP 984A as well as the core-bottoms of NEAP 5B and NEAP 11B (Table 2). Alkenone  
132 samples were purified from total lipid extracts of 37-107 g of freeze-dried homogenized  
133 sediments employing the methods of (Ohkouchi et al., 2005). Samples were extracted  
134 using a Soxhlet apparatus (48 h, dichloromethane:methanol 93:7 v:v). or a Dionex  
135 Accelerated Solvent Extractor (dichloromethane:methanol, 9:1 v:v). Extracts were  
136 subjected to a sequence of wet-chemical techniques including saponification, silica-gel  
137 chromatography, urea adduction and silver nitrate/silica gel chromatography. Yields  
138 and sample purities were checked with a gas chromatograph equipped with a flame  
139 ionization detector (GC/FID). Purified alkenone fractions were quantified with behenic  
140 acid myristyl ester as an external standard. The samples comprising C<sub>37</sub>-, C<sub>38</sub>-, and C<sub>39</sub>-  
141 alkenones were subsequently sealed with copper oxide in pre-combusted evacuated  
142 quartz tubes, and then combusted at 850°C overnight. Resulting CO<sub>2</sub> gas was purified,  
143 quantified and converted to graphite with cobalt as a catalyst for radiocarbon analysis  
144 by AMS. Alkenone samples yielded 26-210 µg carbon and were analyzed using dedicated  
145 techniques for small samples (Pearson et al., 1998).

146 Results of radiocarbon measurements are reported as radiocarbon concentrations  
147 ( $\Delta^{14}\text{C}$ ) and conventional radiocarbon ages (Stuiver & Polach, 1977). Conventional  
148 radiocarbon ages of co-occurring sediment constituents were compared without prior  
149 radiocarbon age calibration. However, foraminiferal ages were calibrated using the

150 online calibration tool CALIB 6.0 (Reimer et al., 2009) and the MARINE09 calibration  
151 curve. Highest probability ages (rounded to the nearest 10 from 0-10.000 a BP and to  
152 the nearest 50 from 10.000-25.000 a BP) were reported as the calibrated age. These  
153 calibrated radiocarbon ages are considered to provide the best estimate of depositional  
154 age of the sediment and are used for the calculation of sediment focussing factors (s.  
155 below).

156

### 157 *Uranium-series analyses*

158 For Uranium (U)-series isotope analyses, 0.3 to 0.4 mg of dried and homogenized  
159 sediment samples from NEAP 5B, 11B, 18B, and ODP 984A were spiked with  $^{229}\text{Th}$  and  
160 dissolved by acid digestion in nitric acid ( $\text{HNO}_3$ ), perchloric acid ( $\text{HClO}_4$ ) and  
161 hydrofluoric acid (HF). The acid digested samples were processed by a procedure for  
162 separation of Th fractions by anion exchange described by (Choi et al., 2001). Briefly, U-  
163 series isotopes were extracted from the total acid digested sample by co-precipitation  
164 with iron oxy-hydroxides (3 times). Precipitates were recovered by centrifugation and  
165 decantation and re-dissolved in hydrochloric acid (HCl). Small aliquots for the  
166 determination of  $^{238}\text{U}/^{232}\text{Th}$  ratios were taken and the remaining solution was eluted  
167 with 12 mL of 9N HCl from an anion exchange column packed with AG1-X8 resin. Th-  
168 containing fractions were evaporated to a small volume and passed through a second  
169 anion exchange column using 8N  $\text{HNO}_3$ . Purified solutions were evaporated to a small  
170 drop, stored in a Teflon screw cap vial and diluted with 0.3 mL MilliQ water prior to  
171 analysis by ICP/MS (Finnigan MAT Element). Concentrations of  $^{230}\text{Th}$  were calculated  
172 from the  $^{230}\text{Th}/^{229}\text{Th}$  ratio (for method details see Choi et al., 2001). Background  
173 corrections were based on analysis of method and column blanks. Excess  $^{230}\text{Th}$   
174 corrected for contribution of  $^{230}\text{Th}$  derived from decay of detrital  $^{238}\text{U}$  was estimated



175 from the measured concentration of  $^{232}\text{Th}$  in the sediment and an assumed average  
176 activity ratio of detrital  $^{238}\text{U}$  to  $^{232}\text{Th}$  of  $R=0.5$  (Henderson and Anderson, 2003;  
177 McManus et al., 1998). A correction for radioactive decay of the unsupported  $^{230}\text{Th}$  with  
178 a half-life of 75.7 ka is made based on the calibrated foraminiferal radiocarbon ages  
179 (François et al., 2004). Ingrown  $^{230}\text{Th}$  from decay of authigenic  $^{234}\text{U}$  is estimated from an  
180 assumed activity ratio of  $^{234}\text{U}$  and  $^{238}\text{U}$  of 1.14 and from the decay equation and the  
181 measured radiocarbon sediment age. The resulting corrected values  $^{230}\text{Th}_{\text{xs0}}$  are then  
182 used for calculation of focussing factors ( $\Psi$ ) and sediment fluxes, employing the  
183 equations given in François (2004). Focussing factors for core intervals were calculated  
184 from  $^{230}\text{Th}_{\text{xs0}}$  inventories divided by the production of  $^{230}\text{Th}$  in the overlying water  
185 column. For this calculation the mean of the  $^{230}\text{Th}_{\text{xs0}}$  values measured at the top and  
186 bottom of these intervals and their respective calibrated foraminiferal radiocarbon ages  
187 as age control were used as well as dry bulk density estimated at  $0.5 \text{ g cm}^{-3}$  for all  
188 samples based on shipboard measurements on parallel ODP core 984B (Jansen et al.,  
189 1996). Values of  $\Psi > 1$  imply the occurrence of sediment focussing by addition of  
190 laterally supplied material, while exclusive particle supply by vertical settling would  
191 result in a  $\Psi$  of 1, and  $\Psi < 1$  indicates some erosion.

192

#### 193 **4) Results**

194 Radiocarbon ages of planktic foraminifera, TOC and alkenones from ODP984 samples  
195 generally increase with depth (Tables 2 and 3. Figure 2). The lowermost foraminifera  
196 sample at 5.05 mbsf sample is 23.1 conventional radiocarbon ka old ( $^{14}\text{C}$  ka hereafter).  
197 In the uppermost 3 mbsf, roughly corresponding to the Holocene core section,  
198 foraminifera and alkenone conventional radiocarbon ages agree within  $1\sigma$  errors ( $2\sigma$  for  
199 the uppermost sample), whereas TOC is on average 900 yr older than co-occurring

200 foraminifera. Below 3 mbsf, age differences between foraminifera and TOC are more  
201 variable and significantly greater (up to 5850 yr). Unfortunately, alkenone  
202 concentrations were too low in this sediment interval to permit radiocarbon dating.

203 NEAP cores 5B and 18B span only the past 2.0 and 2.3 <sup>14</sup>C ka, respectively, whereas  
204 NEAP 11B covers 8.3 <sup>14</sup>C ka (Figure 3). In the two cores from high-accumulation rate  
205 sites (5B and 18B), TOC is 390 to 1020 <sup>14</sup>C yr older than co-occurring foraminifera, while  
206 TOC and foraminifera ages at 11B were identical within error. Compound abundance  
207 only allowed alkenone radiocarbon dates at the core-bottoms of 5B and 11B, which  
208 agreed with foraminifera ages within 2 $\sigma$  and 1 $\sigma$  error margins, respectively.

209 Concentrations of <sup>230</sup>Th<sub>xs</sub> as well as sediment focussing factors ( $\Psi$ ) and fluxes are  
210 presented in Table 4. At stations NEAP 5B and 18B characterized by high sedimentation  
211 rates. Holocene  $\Psi$  values of 4.7 were calculated at both sites. In contrast,  $\Psi$  for the low  
212 accumulation rate core NEAP 11B was 0.6. <sup>230</sup>Th<sub>xs</sub>-corrected sediment fluxes range from  
213 2.4 g m<sup>-2</sup> yr<sup>-1</sup> at the deepest site NEAP 18B to 4.1 g m<sup>-2</sup> yr<sup>-1</sup> at NEAP 11B.

214 The highest focussing factors were calculated for the upper 2 mbsf of ODP984  
215 reaching  $\Psi$  values of 4.5 to 5.1. Normalized fluxes of 2.4 – 3.3 g m<sup>-2</sup> yr<sup>-1</sup> are similar to  
216 those at nearby site NEAP 5B. In contrast, normalized vertical fluxes during the glacial  
217 were higher (3.3-3.7 g m<sup>-2</sup> yr<sup>-1</sup>), while sediment focussing appears to have been lower ( $\Psi$   
218 = 1.7 - 2.4). It has to be noted, though, that the deep circulation of the modern North  
219 Atlantic leads to an export of a proportion of <sup>230</sup>Th produced in the water column that is  
220 estimated to be between 10% and as much as 50% (Yu et al., 1996; Vogler et al., 1998).  
221 This phenomenon has important implications for calculated  $\Psi$ , which would be  
222 depressed by a commensurate amount, resulting in an underestimate of lateral  
223 contribution to the sediment in the Holocene. Moreover, deep-ocean ventilation likely  
224 has varied over the 20 ky timescale of our study. To the extent that the intermediate-

225 depth circulation may have been stronger in the past, the observed differences in  $\Psi$   
226 between Holocene and glacial sediment might in part be explained by these effects.  
227 However, recent evidence suggests that there was little difference between the strength  
228 of the Holocene and glacial circulation at our study location (Praetorius et al., 2008).

229

## 230 **5) Discussion**

### 231 *Age relationships between planktic foraminifera and alkenones*

232 After the discovery of large age offsets between co-occurring planktic foraminifera  
233 and alkenones at Bermuda Rise (Ohkouchi et al., 2002), sediment drifts were suspected  
234 to be particularly prone to temporal and perhaps even spatial decoupling of fine- and  
235 coarse-grained marine constituents deposited at the same time. Unlike at Bermuda Rise,  
236 However, alkenone and planktic foraminiferal radiocarbon ages on Björn Drift agree  
237 well. This is true both for locations with high sedimentation rates (ODP 984 and NEAP  
238 5B) as well as for the off-axis site with lower sediment accumulation rates, NEAP 11B. At  
239 the latter location, currents are expected to be faster, and the sortable silt proxy of the  
240 core-top shows this to be the case (Bianchi and McCave, 2000). Combined with the  
241 compelling morphological, sedimentological, and radionuclide evidence for the  
242 occurrence of sediment focussing at the high-accumulation rate sites, these data indicate  
243 that if alkenones are affected by sediment redistribution at all, the redistribution  
244 processes occur too rapidly to be resolved within the uncertainty range of radiocarbon  
245 dating, i.e., within decades after alkenone formation. This finding is in accordance with  
246 observations by Jonkers et al., (2010), who deduced from sediment trap data from  
247 Gardar Drift that only rapid lateral supply of freshly produced biogenic material can  
248 explain the observed high fluxes to the sediment.

249 Sediment redistribution was shown to be similarly rapid in the Panama Basin (Kusch  
250 et al., 2010), another location at which diverse evidence for sediment redistribution  
251 from various proxies is available. Similarly, in the Argentine Basin, northward transport  
252 of marine organic matter entrained in the Falkland/Malvinas surface current results in  
253 spatial de-coupling of temperatures inferred from alkenones and foraminifera (Benthien  
254 and Müller, 2000; Rühlemann and Butzin, 2006). but no temporal offsets are evident  
255 (Mollenhauer et al., 2006). On the other hand, data from continental margin sediments  
256 suggest that downslope transport of re-suspended shelf sediments involves pre-aged  
257 material resulting in substantial age offsets at sites with organic-rich sediments  
258 (Mollenhauer et al., 2005). Taken together, our new and prior published data suggest  
259 that redistribution of marine organic matter is a widespread process in the ocean, but  
260 the timescales of organic matter transport and sedimentation may vary markedly.  
261 Depending on the sedimentological setting, transport occurs over distances ranging  
262 from less than a hundred to several thousand kilometres, and advected material can  
263 either be fresh or contain pre-aged marine organic matter.

264 Knowing the factors that determine whether or not temporal and spatial decoupling  
265 is likely to occur is of great interest in order to evaluate the suitability of a core site for  
266 high-resolution palaeoenvironmental reconstructions using multiple proxies residing in  
267 different grain size fractions. From comparison of the locations so far investigated for  
268 temporal and spatial offsets between alkenones and planktic foraminifera some likely  
269 factors can be identified.

270 1) Spatial de-coupling of organic proxies compared to foraminifera is to be expected  
271 where a strong gradient from high to low productivity is observed along the flow-path of  
272 a current. These conditions are met in the Argentine Basin, where the Falkland/Malvinas  
273 surface current flows along the South American coast from highly productive Southern

274 Ocean waters to the more oligotrophic subtropical western South Atlantic, and the  
275 bottom current flow is in the same sense. A strong productivity gradient also exists  
276 between the waters overlying the Laurentian Fan and Scotian Margin and those of the  
277 oligotrophic subtropical gyre of the North Atlantic. The former areas are the source for  
278 fine-grained sediment deposited at the Bermuda Rise located beneath the oligotrophic  
279 gyre regions (Englebrecht and Sachs, 2005). However, this material is transported by  
280 the deep-western boundary current and is likely predominantly re-suspended following  
281 benthic storm events (Hollister and McCave, 1984). Since the transported material is re-  
282 suspended, it contains considerable amounts of pre-aged marine organic matter, which  
283 results in large age offsets between foraminifera and alkenones. At the continental  
284 margins of Southwest Africa and Southwest South America, age offsets between  
285 foraminifera and alkenones have been explained by down-slope transport of organic-  
286 rich resuspended sediments, probably caused by internal tides (Mollenhauer et al.,  
287 2003; Mollenhauer et al., 2005). In contrast to the Argentine Basin and the Bermuda  
288 Rise, the transported material deposited at these continental margins sites is likely  
289 derived from sources only a few tens of kilometers apart from the sites of deposition.

290 2) The two locations where no significant age offsets between foraminifera and  
291 alkenones are observed despite strong evidence for sediment focussing, i.e., the Panama  
292 Basin (Kusch et al., 2010), and the Björn and Gardar Drift area investigated in this study,  
293 both are located in deep-sea basins close to and downstream from the ridges bordering  
294 the basins (Carnegie Ridge and Iceland-Faroe Ridge (IFR), respectively). At the same  
295 time, in both basins extensive sediment redistribution is documented by morphological  
296 and proxy evidence. A speculative hypothesis to explain the lack of temporal decoupling  
297 between marine proxies in these regions could be that the ridges and sea-mounts in the  
298 upstream region of the currents bathing the core sites influence and cause the current

299 regime where, on the one hand, small particles are resuspended rapidly after formation  
300 (Turnewitsch et al., 2008), but on the other the same ridges and seamounts might serve  
301 as sediment traps for pre-aged suspended material originating from distal locations on  
302 their current-facing sides. Thus the organic components may be transported to the core  
303 sites quickly without intermediate storage elsewhere, implying that they likely also only  
304 travel over short lateral distances. This was also suggested by Jonkers et al. (2010) to be  
305 the case for biogenic material deposited on Gardar Drift. In the Iceland Basin, the IFR  
306 furthermore is associated with high productivity (in a region of generally high  
307 productivity), which together with the nearby terrestrial sources from Iceland supplies  
308 copious amounts of fresh organic matter, potentially swamping any signal from erosion  
309 and the redistribution of older sediment eroded from between 1450 and 1800 m  
310 (Thornalley et al., 2010).

311

#### 312 *Age offsets between foraminifera and TOC*

313 In contrast to alkenones, TOC is systematically older than co-occurring planktic  
314 foraminifera at all Björn and Gardar Drift sites with high accumulation rates. At the off-  
315 axis site, however. TOC and planktic foraminiferal ages are identical within  $1\sigma$  errors.  
316 This implies that at the latter site, TOC consists of larger fractions of fresh material,  
317 likely predominantly of marine and perhaps local origin as suggested by the  $\delta^{13}\text{C}$  values  
318 of -21.2 and -22.1‰, which are slightly more depleted than typical North Atlantic POM  
319 values (-19‰) (Hall and McCave, 1998). Taking into account the  $\Psi$  value of 0.6 at NEAP  
320 11B, which argues against deposition of pre-aged transported material at this site, the  
321 predominant source of organic matter at this location is likely vertical flux of fresh  
322 particles derived from marine primary production, potentially entrained in coarse-  
323 grained and densely packed fecal pellets, which cannot easily be re-suspended and at

324 the same time provide a high preservation potential for labile organic matter. In  
325 contrast, the age difference between TOC and foraminifera at the other sites coupled  
326 with  $\Psi$  values  $>4$  in the Holocene results from addition of pre-aged material. Since the  
327 alkenones in the same samples agree in age with the foraminifera, the advected pre-aged  
328 organic matter is likely free of or very poor in alkenones. The  $\delta^{13}\text{C}$  values in the  
329 Holocene sediments at the high accumulation rate sites range between -21.0 and  
330 -22.9‰, similar to the values at NEAP 11B, where no sediment focussing is evident and  
331 TOC is likely predominantly derived from marine primary production in the overlying  
332 surface waters. The combined organic geochemical, stable carbon and radiocarbon  
333 isotopic evidence therefore implies redistribution of pre-aged marine organic matter  
334 that contains low to negligible abundances of alkenones. The glacial age (21.7 calibrated  
335 ka BP) sediments in ODP 984A do not contain measurable amounts of alkenones.  
336 Barents Sea slope sediments older than 14.1 ka BP were found to be free of alkenones  
337 (Martrat et al., 2003), and Nordic Sea glacial age sediments are also characterized by  
338 generally low alkenone concentrations (Rosell-Melé and Comes, 1999). Therefore, the  
339 pre-aged organic matter deposited at sites ODP 984 and NEAP 5B and 18B could derive  
340 from glacial-age marine material from near the core site, most likely the erosional  
341 southern slope of the IFR and Faroe Bank Channel (Dorn and Werner, 1993), or from a  
342 heretofore unidentified source.

343

#### 344 *Amount, age and origin of transported organic matter*

345 In the following discussion, we will first focus only on the most recently deposited  
346 sediment (last 2.3 ka), which allows comparison of all four sites investigated in this  
347 study. Here we concentrate on an assessment of the amount and composition of

348 transported organic matter deposited at the core sites using isotopic mass balance  
349 calculation:

$$350 \quad \Delta^{14}\text{C}_{\text{TOC}} = (a \times \Delta^{14}\text{C}_{\text{adv}} + b \times \Delta^{14}\text{C}_{\text{loc}}) / (a + b) \quad \text{Equation 1}$$

351  $\Delta^{14}\text{C}_{\text{TOC}}$  denotes the measured radiocarbon concentration of total organic carbon  
352 corrected for the decay since the time of deposition.  $\Delta^{14}\text{C}_{\text{adv}}$  is the radiocarbon  
353 concentration of the advected and  $\Delta^{14}\text{C}_{\text{loc}}$  that of the locally sourced and vertically  
354 supplied sediment contribution at the time of deposition, i.e., both values are corrected  
355 for the decay that occurred since deposition. Decay-corrected radiocarbon  
356 concentrations of TOC and planktic foraminifera can be calculated from measured  $\Delta^{14}\text{C}$   
357 values using the equation presented by Ohkouchi et al. (2002). The time of deposition is  
358 assumed to be best reflected by the calibrated radiocarbon age of the planktic  
359 foraminifera in each sample. Factors  $a$  and  $b$  are the relative contributions of the  
360 advected and local organic matter, respectively. Focussing factors are regarded as a  
361 means of quantifying the amount of laterally supplied material (i.e., factor  $a$  in Equation  
362 1). In a simplified view, a focussing factor of 4.5 indicates deposition of 4.5 times the  
363 amount of vertically sinking particles, i.e., that the sediment is composed of one part  
364 (23%) vertically sinking particles and 3.5 parts (77%) laterally advected material,  
365 assuming equal composition of both fluxes and  $^{230}\text{Th}$  equilibration of particles with the  
366 water depth of the site of deposition (François et al., 2004). If the measured focussing  
367 factors are used as an estimate of the amount of laterally supplied pre-aged material, 77  
368 to 79 % of the sediment at the drift site samples of the last 2.3 ka (NEAP sites 5B and  
369 18B and uppermost ODP 984 depth interval) would be transported (factor  $a$ ). The  
370 average age at the time of deposition of the transported organic matter can then be  
371 estimated using the mass balance equation (Equation 1) and the assumption that the  
372 radiocarbon concentration of the vertical flux at the time of deposition ( $\Delta^{14}\text{C}_{\text{loc}}$ ) equals



373 the decay-corrected radiocarbon concentrations of planktic foraminifera. This  
374 assumption is valid if the vertical organic matter flux is composed of marine organic  
375 matter produced in the water depth at which the planktic foraminifera thrived. If  
376 Equation 1 is re-arranged and solved for  $\Delta^{14}\text{C}_{\text{adv}}$ , the  $^{14}\text{C}$  age  $t$  of the transported organic  
377 matter at the time of deposition can be derived as

$$378 \quad t = -8033 \times \ln(\Delta^{14}\text{C}_{\text{adv}}/1000 + 1) \quad \text{Equation 2}$$

379 Using this mass balance, the average radiocarbon age of transported organic matter  
380 at the time of deposition is estimated to range from approximately 1020 to 1750  $^{14}\text{C}$   
381 years in the sediments accumulating during the last 2.3 cal ka.

382 In a second independent approach, the amount of transported organic matter ( $a$ ) can  
383 be estimated when assuming its age ( $t$ ) converted to the radiocarbon concentration at  
384 the time of deposition by re-arranging Equation 2 to solve for  $\Delta^{14}\text{C}_{\text{adv}}$  and using again the  
385 mass balance equation (Equ. 1). As before, the assumption is made that the locally  
386 sourced organic matter at the time of deposition has a radiocarbon concentration equal  
387 to the decay-corrected  $^{14}\text{C}$ -concentration of the planktic foraminifera. As discussed  
388 above, the pre-aged transported organic matter could consist of glacial age (18  $^{14}\text{C}$  ka;  
389  $\Delta^{14}\text{C}_{\text{adv}} = -894\text{‰}$ ), or fossil ( $\Delta^{14}\text{C}_{\text{adv}} = -1000\text{‰}$ ), marine organic matter. If we assume  
390 that glacial age or fossil marine organic matter was the only transported material, only  
391 6-13% or 5-12%, respectively, of the sediment accumulating at the drift sites would  
392 consist of this material.

393 If we assume homogenous composition of the transported material, the first mass-  
394 balance calculation requires lateral supply of large amounts of only slightly pre-aged  
395 material. Recent work on the particle affinity of  $^{230}\text{Th}$  as a function of grain-size and  
396 mineralogy suggests that due to preferential sorption on clay-sized particles and  
397 hydrodynamic particle sorting during transport, focussing factors based on bulk

398 sediment  $^{230}\text{Th}_{\text{xs}}$  inventories tend to overestimate the amount of lateral flux  
399 (Kretschmer et al., 2010; McGee et al., 2010). The actual amounts of laterally  
400 transported material supplied to the core sites are likely to be somewhat less than  
401 suggested by focussing factors calculated from bulk sediment samples. This size-bias  
402 would be greatest at NEAP 18B, where grain size is finest (Bianchi and McCave, 2000).  
403 Therefore we do not regard the estimate of 77-79% addition of only slightly pre-aged  
404 material a plausible scenario.

405 On the other hand, the estimate of 5 to 13% of lateral flux generated by the second  
406 mass-balance calculation is insufficient to explain the high sedimentation rates at the  
407 drift sites. Based on the comparison of Holocene sedimentation rates estimated for the  
408 off-axis site NEAP 11B (5 cm/ka) and sites NEAP 5B and 18B (20 cm/ka) as well as ODP  
409 984 (27 cm/ka), a lateral flux of about 75% of the total flux seems realistic. Therefore, in  
410 order to reconcile the  $^{230}\text{Th}_{\text{xs}}$  and radiocarbon data, we suggest that the organic  
411 sediment supplied laterally to our core-sites during the past 2.3 cal ka is composed of a  
412 mixture of fresh local material and 5-13% organic matter free of or very poor in  
413 alkenones and of glacial age or older. As a consequence, alkenone based sea-surface  
414 temperature reconstructions can be interpreted as local signals given this minor  
415 transported bias.

416

#### 417 *Downcore variability in age offsets and focussing factors*

418 A pronounced difference in the age offsets between foraminifera and TOC exists  
419 between the Holocene and glacial age sediments of ODP 984, suggesting that the  
420 advected material was derived from different, even older sources during the glacial than  
421 the Holocene. Glacial age sediments of ODP 984 are characterized by high and variable  
422 age differences between foraminifera and TOC and more  $^{13}\text{C}$ -depleted stable carbon

423 isotopic composition ( $\delta^{13}\text{C}$  values ranging between -23.9 and -24.9 ‰). Indeed, all  
424 samples with large age offsets show  $\delta^{13}\text{C}$  values lower than approximately -23.5‰  
425 (Figure 4), arguing for advection of pre-aged organic matter, which may include pre-  
426 aged terrigenous material or marine organic matter synthesized at low surface water  
427 temperatures (Rau et al., 1989). Higher contributions of terrigenous organic matter to  
428 total TOC burial during the glacial than the Holocene were also reported by Hall and  
429 McCave (1998) for the NW European continental margin. Based on  $C_{\text{org}}/N$  ratios, these  
430 authors argued that increased glacial supply of terrigenous material is the most likely  
431 explanation for the observed isotopic trends in the region. Whether the more  $^{13}\text{C}$ -  
432 depleted TOC in glacial and deglacial sediments is caused by admixture of pre-aged  
433 terrigenous or “cold” marine organic matter cannot be resolved in this study. This does,  
434 however, not affect the interpretation of the  $^{14}\text{C}$  data.

435 The study area is located in higher northern latitudes, which were covered by winter  
436 sea-ice during the last glacial maximum (Sarnthein et al., 2003), and adjacent land-  
437 masses were glaciated. Therefore, supply of glacial-age terrestrial organic matter to the  
438 sediments during the last glacial seems less probable. It is highly likely that glacial  
439 erosion of Iceland and the Faroes mobilized much older terrestrial organic matter, e.g.,  
440 from the last interglacial. If Eemian terrestrial organic matter containing no measurable  
441 radiocarbon (i.e.,  $\Delta^{14}\text{C}_{\text{adv}} = -1000$  ‰ in Equation 1) was supplied to the core location  
442 and caused the large age offsets between foraminifera and TOC prior to the early  
443 Holocene, mass balance calculation suggests that the relative contribution of this  
444 material would be significantly less than 20% of TOC.

445 Sediment focussing factors are lower for glacial age sediments than for the Holocene  
446 ( $\Psi = 1.7$  and  $2.4$ ). North Atlantic intermediate water flow speed between 1.1 and 2km  
447 water depth is reconstructed to be more rapid during the glacial than the Holocene

448 (McCave et al., 1995). Even though data from Björn Drift, where ODP 984 was retrieved,  
449 are lacking from the study of McCave et al. (1995), the evidence for increased flow speed  
450 at the water depth of site 984 stems from locations directly upstream. It thus appears  
451 that increased flow speeds resulted in less sediment focussing at site ODP 984, but  
452 advected material contained a greater proportion of pre-aged organic matter than  
453 during the Holocene. A change in source of the advected material at ODP984 between  
454 the glacial and the Holocene is supported by grain size data (Praetorius et al., 2008).  
455 These authors suggest that, while flow speeds remained at comparable levels between  
456 the glacial and the Holocene, advected material during the Holocene was transported  
457 over much shorter distances thus implying a more proximal sediment source after the  
458 initiation of the Iceland-Scotland Overflow Waters at the onset of the Holocene.

459

## 460 **6) Conclusions**

461 Radiocarbon age differences between alkenones and foraminifera in Holocene sediment  
462 drifts of the Iceland Basin were negligible, implying that redistribution of sediments  
463 within the basin is rapid and occurs soon after formation of marine organic matter, or  
464 that transported material contains negligible amounts of alkenones. Pre-aged organic  
465 material supplied during the Holocene to the core-sites is likely fossil or at least of  
466 glacial age but only accounts for less than 12% of TOC. Our data are consistent with  
467 redistribution of particles consisting of a mixture of fresh and pre-aged material.  
468 Downcore variations in age offsets between foraminifera and TOC document changes in  
469 source area of the transported material between the glacial and the Holocene. Focussing  
470 factors based on  $^{230}\text{Th}_{\text{xs}}$  cannot be used directly to provide a unique determination of the  
471 amount of pre-aged organic matter. However, lateral mixing does not always hinder the  
472 use of multiple proxies from a single core in reconstructing palaeoenvironmental

473 change. In order to better constrain source, age and amount of transported material,  
474 multiproxy studies including biomarker information on organic matter composition,  
475 grain-size spectra of sediments, and multiple isotopes of organic matter should be  
476 considered.

477

## 478 **Acknowledgements**

479 Technical support was provided by Alan Fleer. Susan Brown-Leger and Daniel  
480 Montluçon. The NOSAMS staff is thanked for the radiocarbon analyses. Thoughtful  
481 comments from two anonymous reviewers helped to improve the manuscript. This  
482 work was funded by NSF grant # OCE-0327405 and a WHOI-NOSAMS postdoctoral  
483 scholarship as well as a HGF young investigators group grant to GM. The work was also  
484 supported in part by NSF grants #OCE 0549111 and #OCE 0840430 and an award from  
485 the Comer Research and Education Foundation to JFM. TW gratefully acknowledges the  
486 Royal Society-Wolfson Research Merit Award.

487

## 488 **References**

- 489 Benthien, A., Müller, P.J., 2000. Anomalously low alkenone temperatures caused by lateral  
490 particle and sediment transport in the Malvinas Current region, western Argentine  
491 Basin. *Deep-Sea Research I* 47, 2369-2393.
- 492 Bianchi, G.G., McCave, I.N., 2000. Hydrography and sedimentation under the deep western  
493 boundary current on Björn and Gardar Drifts, Iceland Basin. *Marine Geology* 165, 137-  
494 169.
- 495 Choi, M.S., François, R., Sims, K., Bacon, M.P., Brown-Leger, S., Fleer, A.P., Ball, L.,  
496 Schneider, D., Pichat, S., 2001. Rapid determination of  $^{230}\text{Th}$  and  $^{231}\text{Pa}$  in seawater by  
497 desolvated micro-nebulization Inductively Coupled Plasma magnetic sector mass  
498 spectrometry. *Marine Chemistry* 76, 99-112.
- 499 Dorn, W.U., Werner, F., 1993. The contour-current flow along the southern Iceland-Faeroe  
500 Ridge as documented by its bedforms and asymmetrical channel fillings. *Sedimentary  
501 Geology* 82, 47-59.
- 502 Englebrecht, A.C., Sachs, J.P., 2005. Determination of sediment provenance at drift sites  
503 using hydrogen isotopes and unsaturation ratios in alkenones. *Geochimica et  
504 Cosmochimica Acta* 69, 4253-4265.
- 505 Flood, R.D., Hollister, C.D., 1974. Current-controlled topography on the continental margin  
506 off the eastern United States, in: Burke, C.A., Drake, C.L. (Eds.), *The Geology of  
507 Continental Margins*. Springer Verlag, New York, pp. 197-205.

508 François, R., Frank, M., Rutgers van der Loeff, M.M., Bacon, M.P., 2004.  $^{230}\text{Th}$   
509 normalization: An essential tool for interpreting sedimentary fluxes during the late  
510 Quaternary. *Paleoceanography* 19, doi:10.1029/2003PA000939.

511 Hall, I.R., McCave, I.N., 1998. Glacial-interglacial variation in organic carbon burial on the  
512 slope of the N.W. European Continental Margin. *Progress in Oceanography* 42, 37-60.

513 Henderson, G.M., Anderson, R.F., 2003. The U-series toolbox for paleoceanography.  
514 *Reviews in Mineralogy and Geochemistry* 52, 493-531.

515 Hollister, C.D., McCave, I.N., 1984. Sedimentation under deep-sea storms. *Nature* 309, 220-  
516 225.

517 Jansen, E., Raymo, M.E., Blum, P., al., e., 1996. Proceedings ODP, Initial Reports, 162.  
518 Ocean Drilling Program, College Station, TX.

519 Jonkers, L., Mienis, F., Boer, W., Hall, I.R., Brummer, G.-J.A., 2010. Intra-annual variability  
520 of extremely rapid sedimentation onto Gardar Drift in the northern North Atlantic. *Deep*  
521 *Sea Research Part I: Oceanographic Research Papers* 57, 1027-1038.

522 Kienast, S.S., Kienast, M., Mix, A., Calvert, S.E., François, R., 2007. Thorium-230  
523 normalized particle flux and sediment focusing in the Panama Basin region during the  
524 last 30,000 years. *Paleoceanography* 22, PA2213.

525 Kretschmer, S., Geibert, W., Rutgers van der Loeff, M.M., Mollenhauer, G., 2010. Grain size  
526 effects on  $^{230}\text{Th}_{\text{xs}}$  inventories in opal-rich and carbonate-rich marine sediments. *Earth*  
527 *and Planetary Science Letters* 294, 131-142.

528 Kusch, S., Eglinton, T.I., Mix, A., Mollenhauer, G., 2010. Timescales of lateral sediment  
529 transport in the Panama Basin as revealed by compound-specific radiocarbon ages of  
530 alkenones. *Earth and Planetary Science Letters* 290, 340-350.

531 Marcantonio, F., Anderson, R.F., Higgins, S.M., Stute, M., Schlosser, P., Kubik, P., 2001.  
532 Sediment focusing in the central equatorial Pacific ocean. *Paleoceanography* 16, 260-  
533 267.

534 Martrat, B., Grimalt, J.O., Villanueva, J., van Kreveld, S., Sarnthein, M., 2003. Climatic  
535 dependence of the organic matter contributions in the north eastern Norwegian Sea over  
536 the last 15,000 years. *Organic Geochemistry* 34, 1057-1070.

537 McCave, I.N., 1994. Cruise Report, RRS Charles Darwin Cruise 88, NEAPACC, in:  
538 *Sciences, Department of Sciences, University of Cambridge*, 45 pp.

539 McCave, I.N., 2002. A poisoned chalice? *Science* 298, 1186-1187.

540 McCave, I.N., Manighetti, B., Beveridge, N.A.S., 1995. Circulation in the glacial North  
541 Atlantic inferred from grain-size measurements. *Nature* 374, 149-152.

542 McCave, I.N., Tucholke, B.E., 1986. Deep current-controlled sedimentation in the western  
543 North Atlantic, in: Vogt, P.R., Tucholke, B.E. (Eds.), *The Geology of North America*,  
544 Volume M, The Western North Atlantic Region. The Geological Society of America,  
545 pp. 451-468.

546 McGee, D., Marcantonio, F., McManus, J. F., and Winkler, G., 2010. The response of excess  
547  $^{230}\text{Th}$  and extraterrestrial  $^3\text{He}$  to sediment redistribution at the Blake Ridge, western  
548 North Atlantic. *Earth and Planetary Science Letters* 299, 138-149.

549 McManus, J.F., Anderson, R.F., Broecker, W.S., Fleisher, M.Q., Higgins, S.M., 1998.  
550 Radiometrically determined sedimentary fluxes in the sub-polar North Atlantic during  
551 the last 140,000 years. *Earth and Planetary Science Letters* 155, 29-43.

552 McNichol, A.P., Osborne, E.A., Gagnon, A.R., Fry, B., Jones, G.A., 1994. TIC, TOC, DIC,  
553 DOC, PIC, POC - unique aspects in the preparation of oceanographic samples for  $^{14}\text{C}$ -  
554 AMS. *Nuclear Instruments and Methods in Physics Research B* 92, 162-165.

555 Mollenhauer, G., Eglinton, T.I., Ohkouchi, N., Schneider, R.R., Müller, P.J., Grootes, P.M.,  
556 Rullkötter, J., 2003. Asynchronous alkenone and foraminifera records from the  
557 Benguela Upwelling System. *Geochimica et Cosmochimica Acta* 67, 2157-2171.

558 Mollenhauer, G., Kienast, M., Lamy, F., Meggers, H., Schneider, R.R., Hayes, J.M., Eglinton,  
559 T.I., 2005. An evaluation of  $^{14}\text{C}$  age relationships between co-occurring foraminifera,  
560 alkenones, and total organic carbon in continental margin sediments. *Paleoceanography*  
561 20, PA1016; doi:10.1029/2004PA001103.

562 Mollenhauer, G., McManus, J.F., Benthien, A., Müller, P.J., Eglinton, T.I., 2006. Rapid  
563 lateral particle transport in the Argentine Basin: Molecular  $^{14}\text{C}$  and  $^{230}\text{Th}_{\text{xs}}$  evidence.  
564 *Deep Sea Research Part I: Oceanographic Research Papers* 53, 1224-1243.

565 Ohkouchi, N., Eglinton, T.I., Hughen, K., Roosen, E., Keigwin, L.D., 2005. Radiocarbon  
566 dating of alkenones from marine sediments: III. Influence of solvent extraction  
567 procedures on  $^{14}\text{C}$  measurements of foraminifera. *Radiocarbon* 47, 425-432.

568 Ohkouchi, N., Eglinton, T.I., Keigwin, L.D., Hayes, J.M., 2002. Spatial and temporal offsets  
569 between proxy records in a sediment drift. *Science* 298, 1224-1227.

570 Pearson, A., McNichol, A., Schneider, R.J., von Reden, K.F., Zheng, Y., 1998. Microscale  
571 AMS  $^{14}\text{C}$  measurement at NOSAMS. *Radiocarbon* 40, 61-75.

572 Praetorius, S.K., McManus, J.F., Oppo, D.W., Curry, W.B., 2008. Episodic reductions in  
573 bottom-water currents since the last ice age. *Nature Geoscience* 1, 449-452.

574 Rau, G.H., Takahashi, T., Marais, D.J.D., 1989. Latitudinal variations in plankton  $[\delta]^{13}\text{C}$ :  
575 implications for  $\text{CO}_2$  and productivity in past oceans. *Nature* 341, 516-518.

576 Reimer, P.J., Baillie, M.G.L., Bard, E., Bayliss, A., Beck, J.W., Blackwell, P.G., Bronk  
577 Ramsey, C., Buck, C.E., Burr, G.S., Edwards, R.L., Friedrich, M., Grootes, P.,  
578 Guilderson, T., Hajdas, I., Heaton, T.J., Hogg, A.G., Hughen, K.A., Kaiser, K.F.,  
579 Kromer, B., McCormac, F.G., Manning, S., Reimer, R.W., Richards, D.A., Southon,  
580 J.R., Talamo, S., Turney, C.S.M., van der Plicht, J., Weyhenmeyer, C.E., 2009. IntCal09  
581 and Marine09 radiocarbon age calibration curves, 0–50,000 years cal BP. *Radiocarbon*  
582 51, 1111-1150.

583 Rosell-Melé, A., Comes, P., 1999. Evidence for a warm Last Glacial Maximum in the Nordic  
584 seas or an example of shortcomings in  $U^{K'}_{37}$  and  $U^K_{37}$  to estimate low sea surface  
585 temperature? *Paleoceanography* 14, 770-776.

586 Rühlemann, C., Butzin, M., 2006. Alkenone temperature anomalies in the Brazil-Malvinas  
587 Confluence area caused by lateral advection of suspended particulate material.  
588 *Geochemistry, Geophysics, Geosystems*, G3 7, Q10015.

589 Sarnthein, M., Pflaumann, U., Weinelt, M., 2003. Past extent of sea ice in the northern North  
590 Atlantic inferred from foraminiferal paleotemperature estimates. *Paleoceanography* 18,  
591 1047.

592 Thomsen, C., Schulz-Bull, D.E., Petrick, G., Duinker, J.C., 1998. Seasonal variability of the  
593 long-chain alkenone flux and the effect on the  $U^{K'}_{37}$ -index in the Norwegian Sea.  
594 *Organic Geochemistry* 28, 311-323.

595 Thornalley, D.J.R., Elderfield, H., McCave, I.N., 2010. Intermediate and deep water  
596 paleoceanography of the northern North Atlantic over the past 21,000 years.  
597 *Paleoceanography* 25, PA1211.

598 Turnewitsch, R., Reyss, J.-L., Nycander, J., Waniek, J.J., Lampitt, R.S., 2008. Internal tides  
599 and sediment dynamics in the deep sea--Evidence from radioactive  $^{234}\text{Th}/^{238}\text{U}$   
600 disequilibria. *Deep Sea Research Part I: Oceanographic Research Papers* 55, 1727-1747.

601 Yu, E.-F., Francois, R., and Bacon, M. P., 1996. Similar rates of modern and last-glacial  
602 ocean thermohaline circulation inferred from radiochemical data. *Nature* 379, 689-694.  
603  
604

605 Table 1: Core locations and estimated thickness of Holocene sediment sequence (NEAP  
 606 cores. see (Bianchi and McCave, 2000))  
 607

Core	Latitude (°N)	Longitude (°W)	Water depth (m)	Holocene thickness (m)
ODP984	61°26'N	24° 5'W	1649	2.7
NEAP 5B	61°04.50'	24°31.76'	1826	2
NEAP 11B	59°47.49'	22°39.24'	2484	0.5
NEAP 18B	54°41.56'	28°21.02'	2879	2



608 Table 2: Radiocarbon concentrations and ages of TOC, alkenones and planktic foraminifera. For foraminiferal radiocarbon dates. *G.*  
 609 *bulloides* were picked (*N. pachyderma* sinistral below 3.55 mbsf (ODP 984 A1A3 samples)).

610

Core	Depth interval	Depth	$\delta^{13}\text{C}_{\text{org}}$	$\Delta^{14}\text{C}$			Conventional radiocarbon age			Calibrated age	
				TOC	alkenones	foraminifera	TOC	alkenones	foraminifera	foraminifera	
	(cm)	(mbsf)	(‰ PDB)	(‰)	(‰)	(‰)	(yr BP)	(yr BP)	(yr BP)	1 $\sigma$ range	age
ODP984A1W1	50-60	0.55	-22.1	-298.5	-262.9	-237.6	2790±45	2400±100	2120±30	1659-1767	1700
ODP984A1W1	100-110	1.05	-22.6	-414.4	-368.0	-369.6	4240±160	3630±110	3650±35	3495-3608	3560
ODP984A1W2	50-60	2.05	-22.5	-616.4	-589.7	-580.8	7640±50	7100±120	6930±45	7402-7486	7420
ODP984A1W2	100-110	2.55	-22.9	-704.4	-666.3	-662.2	9740±50	8760±140	8660±50	9272-9406	9360
ODP984A1A3	50-60	3.55	-23.9	-896.8		-862.3	18200±95		15850±75	18589-18741	18650
ODP984A1A3	100-110	4.05	-23.9	-935.8		-902.8	22000±200		18650±100	21575-21996	21700
NEAP 5B	surface		-21.0	-153.0		-91.3	1280±30		715±30	312-406	355
NEAP 5B	36-38		-21.8	-268.6	-285.2	-232.4	2460±25	2640±360	2070±35	1589-1694	1645
NEAP 11B	surface		-21.2	-643.3		-213.5	1860±25		1880±25	1380-1471	1405
NEAP 11B	37-39		-22.1	-212.2	-655.4	-645.9	8230±40	8510±310	8290±35	8785-8940	8870
NEAP 18B	surface		-21.3	-196.4		-88.4	1700±40		690±30	289-375	310
NEAP 18B	35-37		-21.4	-291.9		-253.9	2720±35		2300±30	1867-1953	1905

611 Table 3: ODP 984C radiocarbon data. Foraminifera radiocarbon dates were obtained on  
 612 monospecific samples of *G. bulloides* (top to 2.835 mbsf) and *N. pachyderma* l. (below  
 613 2.84 mbsf).

614

Core	Depth interval	Depth (mbsf)	$\delta^{13}\text{C}_{\text{org}}$ ‰ VPDB	Conventional radiocarbon age		Calibrated age	
				TOC (yr BP)	foraminifera (yr BP)	1 $\sigma$ range	age
ODP984C1H1	28-30	0.28	-22.0	2120			
ODP984C1H1	30-32	0.30			1440±35	940-1029	970
ODP984C1H1	58-60	0.59			2200±40	1743-1854	1810
ODP984C1H1	60-62	0.60	-22.6	3170			
ODP984C1H1	94-96	0.95	-22.7	4430	3690±40	3550-3667	3610
ODP984C1H1	120-122	1.21	-23.0	5220			
ODP984C1H1	122-124	1.23			4380±40	4441-4576	4520
ODP984C1H2	12-14	1.63			5670±45	6009-6148	6095
ODP984C1H2	14-16	1.64	-22.6	6460			
ODP984C1H2	44-46	1.94	-23.1	7740	6830±65	7293-7412	7370
ODP984C1H2	64-66	2.14	-23.3	8680	7390±50	7808-7919	7850
ODP984C1H2	103-104	2.535			8730±55	9354-9473	9420
ODP984C1H2	104-106	2.54	-23.3	9790			
ODP984C1H2	123-124	2.735			9360±45	10161-10237	10200
ODP984C1H2	124-126	2.74	-24.2	10350			
ODP984C1H2	133-134	2.835			9410±55	10187-10319	10250
ODP984C1H2	134-136	2.84	-24.1	10350			
ODP984C1H2	144-146	2.94	-23.6	11150	11600±55	13056-13187	13100
ODP984C1H3	8-10	3.08	-24.0	14750	11650±110	13064-13277	13150
ODP984C1H3	34-36	3.34	-23.8	17000	15500±60	18088-18298	18200
ODP984C1H3	44-46	3.44	-24.2	20800	16250±90	18795-19377*	18900
ODP984C1H3	80-82	3.8	-24.0	21600	17850±100	20486-21008	20700
ODP984C1H3	104-106	4.04	-23.8	19950	18500±80	21402-21746	21500
ODP984C1H3	140-142	4.4	-24.9	25800	19950±80	23217-23626	23400
ODP984C1H4	8-10	4.58	-24.0	21600			
ODP984C1H4	14-16	4.65			21000±90	24417-24779	24500
ODP984C1H4	40-42	4.9	-24.9	22400	23100±100	26877-27909 <sup>a</sup>	
ODP984C1H4	54-56	5.05			23100±110	26870-27915 <sup>a</sup>	

615 <sup>a</sup>2 $\sigma$  range

616

617 Table 4:  
 618  $^{230}\text{Th}_{\text{xs}}$  corrected for decay and assuming a  $^{238}\text{U}/^{232}\text{Th}$  ratio of  $R=0.5$ , sediment focussing  
 619 factors assuming dry bulk density of  $0.5 \text{ g cm}^{-3}$ , and  $^{230}\text{Th}$  normalized sediment fluxes.  
 620

Core	Depth interval (cm)	Calibrated age	$^{230}\text{Th}_{\text{xs0}}$ (dpm/g)	Focussing factor <sup>a</sup> $\Psi$	Normalized flux ( $\text{g m}^{-2} \text{ yr}^{-1}$ )
ODP984A1W1	50-60	1700	1.36	4.5	3.2
ODP984A1W1	100-110	3560	1.57	5.1	2.8
ODP984A1W2	50-60	7420	1.87	5.1	2.4
ODP984A1W2	100-110	9360	1.62	1.7	2.7
ODP984A1A3	50-60	18650	1.20	2.4	3.7
ODP984A1A3	100-110	21700	1.34		3.3
NEAP 5B	surface	355	1.64		3.0
NEAP 5B	36-38	1645	1.58	4.7	3.1
NEAP 11B	surface	1405	1.61		4.1
NEAP 11B	37-39	8870	1.77	0.6	3.8
NEAP 18B	surface	310	3.06		2.4
NEAP 18B	35-37	1905	3.08	4.7	2.4

621 <sup>a</sup> Focussing factors refer to the interval between this line and the next line (e.g.. interval  
 622 from 50-60 cm (top) to 100-110 cm (bottom) in first line)  
 623

624 Figure captions:

625

626 Figure 1: Study area and core locations. Depth contours (black lines: 1000 m, 2000 m,  
627 3000 m) are at 200 m intervals below 1000 m.

628

629 Figure 2: Conventional radiocarbon ages of ODP site 984 (upper panel) and age  
630 differences between organic sediment constituents (TOC, alkenones) and planktic  
631 foraminifera (lower panel). Error bars in upper panel denote  $1\sigma$  errors of conventional  
632  $^{14}\text{C}$  ages.

633

634 Figure 3: Conventional radiocarbon ages of NEAP box core samples (upper panels) and  
635 age differences between organic sediment constituents (TOC, alkenones) and planktic  
636 foraminifera (lower panels). Error bars in upper panels denote  $1\sigma$  errors of  
637 conventional  $^{14}\text{C}$  ages. At sites NEAP 5B and NEAP 18B, Holocene sediments are  
638 approximately 2 m thick, whereas at NEAP 11B, only  $\sim 0.5$  m of Holocene sediments are  
639 found. Note the different vertical scales on top panels.

640

641 Figure 4: Differences in conventional radiocarbon ages of TOC and planktic foraminifera  
642 plotted against the  $\delta^{13}\text{C}$  values of TOC. Age differences of more than  $\sim 1000$  years are  
643 associated with lower  $\delta^{13}\text{C}$  values indicating a significant contribution of pre-aged  
644 terrigenous organic matter.

645

646

647

648

## Research Highlights

- Sediment supply to NE Atlantic drift sediments occurs rapidly after particle formation
- Lateral mixing does not always hinder multi-proxy palaeoenvironmental reconstruction
- Combined radiocarbon and  $^{230}\text{Th}$  data elucidate temporal changes in sediment provenance

Figure 1

[Click here to download Figure: Figure1\\_Mollenhauer et al.pdf](#)

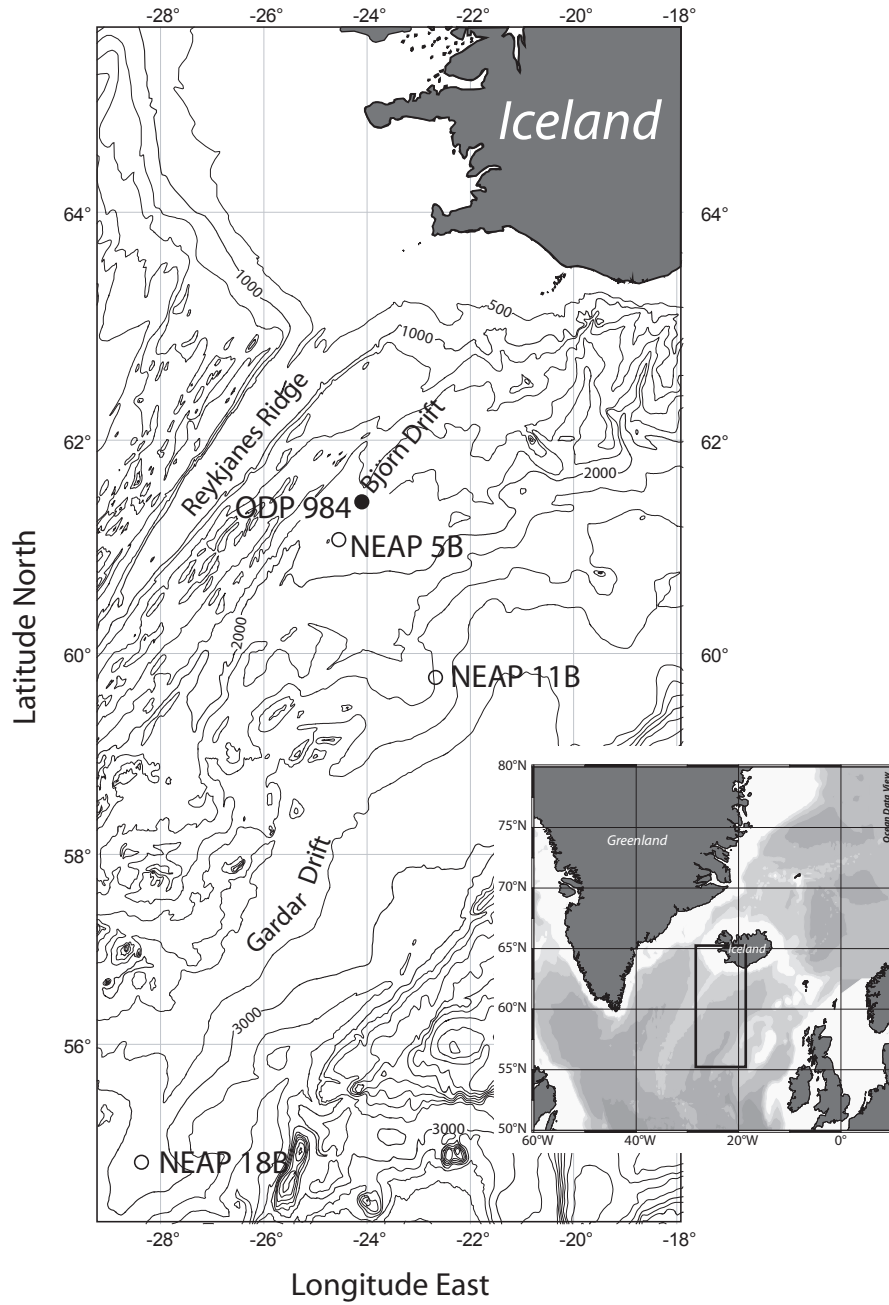


Figure 2

[Click here to download Figure: Figure 2\\_Mollenhauer et al.pdf](#)

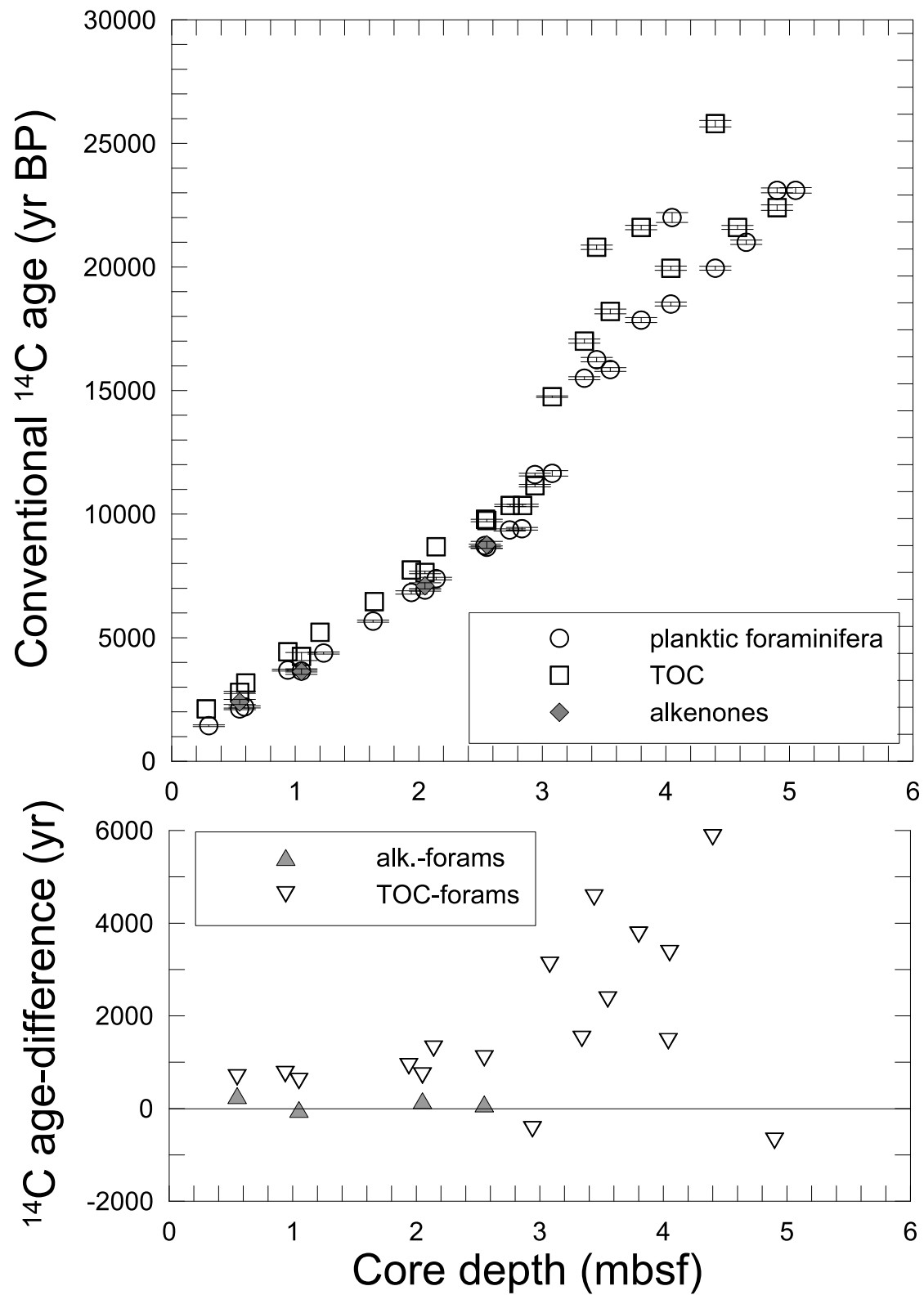


Figure 3

[Click here to download Figure: Figure 3\\_Mollenhauer et al.pdf](#)

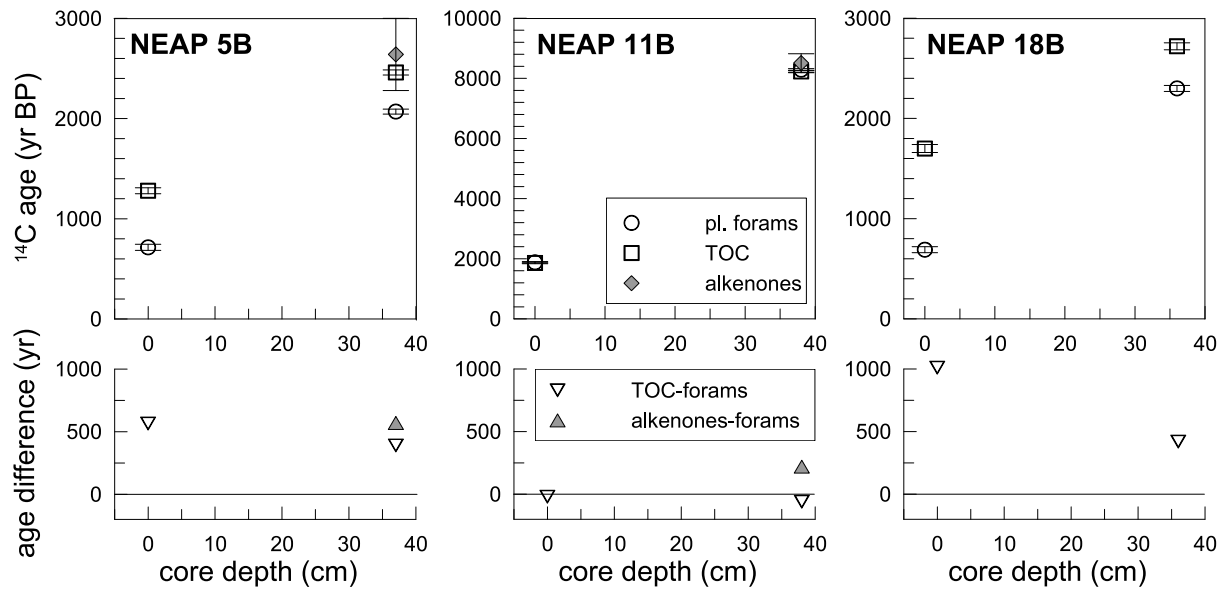




Figure 4

[Click here to download Figure: Figure4\\_Mollenhauer et al.pdf](#)

